International Journal of
**Ocean
System
Engineering**

Numerical And Experimental Studies On Wing In Ground Effect[†]

Sungbu Suh[1,] KwangHyo Jung[1]* and Ho Hwan Chun[2]

[1]Dept. of Naval Architecture and Ocean Engineering, Dong-Eui University, Busan, 614-714, Korea

[2]Dept. of Naval Architecture and Ocean Engineering, Pusan National University, Busan, 609-735, Korea

Abstract

Numerical and experimental studies were performed to investigate the aerodynamic performance of a thin wing in close vicinity to the ground.   The vortex lattice method (VLM) was utilized to simulate the wing in ground (WIG) effect, which included freely deforming wake elements.   The numerical results acquired through the VLM were compared to the experimental results. The experiment entailed varying the ground clearance using the DHMTU (Department of Hydromechanics of the Marine Technical University of Saint Petersburg) wing and the WIG craft model in the wind tunnel.   The aero-dynamic influence of the design parameters, such as angles of attack, aspect ratios, taper ratios, and sweep angles were studied and compared between the numerical and experimental results associated with the WIG craft.   Both numerical and experimental results suggested that the endplate augments the WIG effect for a small ground clearance.   In addition, the vortex lattice method simulated the wake deformation following the wing in the influence of the ground effect.

Keywords: Vortex lattice method (VLM), Wing in ground (WIG) effect, WIG craft

1. Introduction

Several types of high speed ships have been developed in order to meet the increasing demand of transporting high value items and passengers. The wing in ground (WIG) effect craft is a high speed marine transportation vehicle that applies the aerodynamic concept to the ship.   Reportedly, WIG effect improves the aerodynamic efficiency of a vehicle at low altitudes above the water or on ground level.   The efficiency of the WIG craft is better than that of an airplane and much faster than the conventional high speed ship.   The WIG craft exhibits the favourable characteristics of both a ship and an aircraft; thus, the WIG craft is expected to be a future super-high speed marine craft.   The WIG craft covers the triangular zone in the Von Karman-Gabrielli diagram, which presents the transportation efficiency diagram.   The WIG craft fulfils a new category of

high speed transportation between the marine ship and the airplane.   The expectation exists that the WIG craft will be developed in the near future for fast marine transportation in the form of a passenger ship, a cargo/container vessel, a marine leisure craft, a rescue ship, and a military ship.   In addition, the International Maritime Organization (IMO) approved interim guidelines for the WIG craft in December 2002, which is intended to provide as much guidance as possible to those involved in the design, construction, and operation of the WIG craft.

The development of the WIG craft has been ongoing in several countries including Australia, China, Germany, Japan, Korea, and Russia.   In order to design and construct WIG crafts, it was conceptually studied by Kang (2005), Chun et al. (1997), Shin et al. (1997), Sinitsyn (1996), Fuwa et al. (1995), Kuhmstedt (1996), Kirillovikh (1995), and Kubo (1991).   Halloran and O'Meara (1999) reviewed the advantages of the WIG craft and the technical requirements for the military sector.   Many numerical and experimental studies on the ground effect of

---
*Corresponding author. Tel.: +82-51-890-2592, Fax.: +82-51-890-1234.
E-mail address: khjung@deu.ac.kr

wings have been conducted by many researchers: Fink and Lastinger (1961), Carter (1961), Nuhait and Mook (1889), Mizutani and Suzuki (1993), Chun and Chang (2002), and Ahmed and Sharma (2005). Jung et al. (2008) published an extensive experimental report for NACA6409 section tested in the wind tunnel including the flow visualization near the wing body using smoke trace test. The vortex lattice method was used to simulate a freely deforming wake for a lifting surface close to the ground (Katz, 1985). Konstadinopoulos et al. (1985) and Nuhait and Mook (1989) performed a numerical study on the unsteady ground effect for delta and planar wings using VLM.

2. Numerical model – vortex lattice method

To define the wing or craft in the ground effect, two coordinate systems were used for the body-fixed coordinate (o-xyz) on the wing and the inertial coordinate (O-XYZ) in the space, respectively, as shown in fig. 1. The origin of the inertial coordinate coincides with that of the body-fixed coordinate before setting into motion. The kinematic velocity of a wing is defined in the following equation:
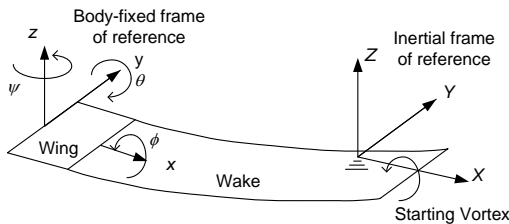

Fig. 1. Inertial and body coordinates system

$$\vec{v} = -\left(\overrightarrow{V_O} + \overrightarrow{v_r} + \vec{\Omega} \times \vec{r}\right) \tag{1}$$

$$\overrightarrow{V_O} = \left(V_{x_o}, V_{y_o}, V_{z_o}\right): \text{Velocity of the origin of}$$
body-fixed frame

$$\vec{v} = \left(v_x, v_y, v_z\right): \text{Velocity in the body-fixed frame}$$

$$\vec{\Omega} = (\phi, \theta, \psi): \text{Rotation of the body-fixed frame}$$

$$\vec{r} = (x, y, z): \text{Position vector}$$

The time derivative in the body-fixed frame system can be obtained by the chain rule.

$$\frac{\partial}{\partial t_{inertial}} = -\left(\overrightarrow{V_o} + \vec{\Omega} \times \vec{r}\right) \bullet \left(\frac{\partial}{\partial x}, \frac{\partial}{\partial y}, \frac{\partial}{\partial z}\right) + \frac{\partial}{\partial t_{body}} \tag{2}$$

The fluid was assumed to be inviscid, irrotational, and incompressible. Therefore, a velocity potential $\Phi(R,t)$ in the inertial frame satisfied the continuity equation:

$$\nabla_R^2 \Phi = 0 \tag{3}$$

The velocity potential was also satisfied in the body-fixed frame as given below:

$$\nabla_r^2 \Phi = 0 \tag{4}$$

The boundary conditions are
No penetration condition across the body boundary:

$$\left(\nabla\Phi + \vec{v}\right) \cdot \hat{n} = 0 \tag{5}$$

Boundary condition at infinity;

$$\nabla\Phi_{r\to\infty} = 0 \tag{6}$$

Since the angular momentum does not change in the potential flow region (Kelvin's theorem), the circulation Γ around a fluid curve enclosing the wing and its wakes have to be conserved:

$$\frac{d\Gamma}{dt} = 0 \tag{7}$$

The flow past the wing was assumed to separate only along the trailing edge. Therefore, the Kutta Condition had to be satisfied along the trailing edge.

$$\nabla\Phi < \infty \text{ at the trailing edge} \tag{8}$$

The general solution of equations (3)~(8) can be obtained by Green's theorem as a doublet and source distribution over the boundary S including the wing surface and the wake.

$$\Phi(x, y, z, t) = -\frac{1}{2\pi} \int_{wing+wake} \left[\Phi \frac{\partial}{\partial n} \frac{1}{r} - \frac{1}{r} \frac{\partial \Phi}{\partial n} \right] dS \tag{9}$$

The first term signifies the doublet distribution and also represents a vortex element (Hess, 1972). The induced velocity $\Delta\vec{q}$ at a point (x,y,z) due to the vortex element dl at (x_o, y_o, z_o) with the circulation (Γ) can be expressed by the Biot-Savart law (Eq. 10)

$$\Delta\vec{q}(x, y, z) = -\frac{1}{4\pi} \Gamma(x, y, z) \frac{r \times dl}{|r|^3} \tag{10}$$

The second term of Eq. (9) represents the source distribution on the thickness along the wing section. For the thin lifting problem, it can be neglected and then the solution can be obtained based only on the vortex distribution. The unsteady vortex lattice method using the solution of Eq. (9) satisfies the governing equation, Eq. (3), and the boundary condition, Eq. (6), at infinity. Therefore, the wing surface was defined by bound vortex rings and the wake was simulated by freely moving vortex rings.
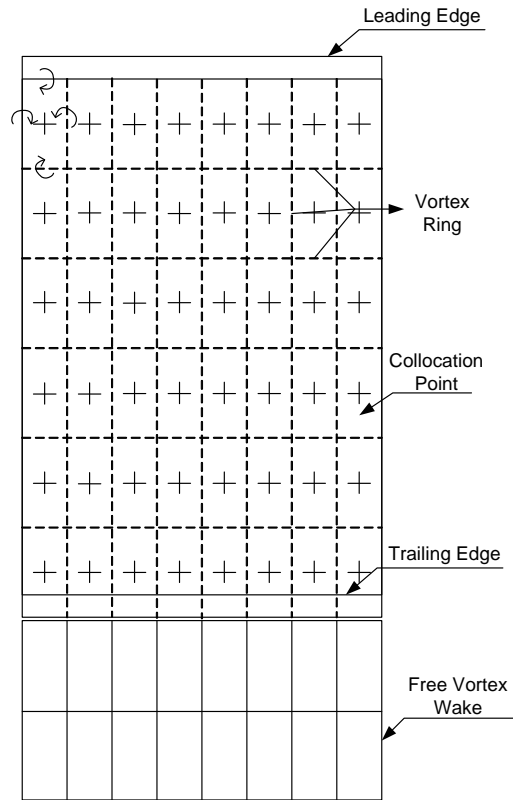

Fig. 2. Vortex lattice for a planar wing

To model the wing geometry including the endplate, vortex ring elements were distributed as shown in Fig. 2. The leading segments of the bound vortex were placed at the quarter chord of each panel. The collocation points were located at the three quarter chord of each panel, which coincided with the center of the vortex ring. The boundary condition, Eq. (5), had to be satisfied at each collocation point. The corner points of the wake vortex ring were calculated at each time step, and the strength of the most recently shed wake (Γ_W) was equal to the strength of the shedding vortex at the trailing edge. The wing surface was composed of panel elements and the boundary condition was applied on the collocation point of each panel element. Then, a set of linear equations was developed as follows:

$$\left[A_{i,j}\right]\left[\Gamma_k\right]=\left[DW_k\right]-\left[WW_k\right] \tag{11}$$

[$A_{i,j}$]: Influence matrix

[DW_k]: Normal velocity term at the collocation points induced by U∞

[WW_k]: Normal velocity term at the collocation points resulting from wake elements

k: Number of collocation points

The influence matrix [$A_{i,j}$] was obtained by the wing geometry and the matrix [WW_k] was determined for each time step. The force free vortex wake was separated at the trailing edge of wing and simulated by detached vortex ring segments at each time step. The pressure difference of each panel was determined by applying the unsteady Bernoulli equation, Eq. (12).

$$\Delta p = p_l - p_u = \rho\left[\left(\frac{Q_t^2}{2}\right)_u - \left(\frac{Q_t^2}{2}\right)_l + \left(\frac{\partial\Phi}{\partial t}\right)_u - \left(\frac{\partial\Phi}{\partial t}\right)_l\right] \tag{12}$$

where Q_t is a tangential velocity due to the wing vortices, u and l represents upper and lower wing surfaces, respectively.

The resulting force on each panel can be calculated by Eq. (13)

$$\Delta\overrightarrow{F_k} = -\left(\Delta p\,\Delta S\right)_k\overrightarrow{n_k} \tag{13}$$

From the resulting force, the lift and induced drag coefficients were obtained by integration along the wing surface

$$C_L = \frac{\sum_{j=1}^{K}\Delta F_j\cos\alpha_j}{0.5\,\rho\,U_\infty^2 S}, \qquad C_{Di} = \frac{\sum_{j=1}^{K}\Delta F_j\sin\alpha_{ij}}{0.5\,\rho\,U_\infty^2 S} \tag{14~15}$$

where α_j and α_{ij} are the angle of attack and the in-

duced angle due to wake-induced downwash of each panel, respectively.

3. Experimental set-up

Experiments were carried out in the wind tunnel at Pusan National University. The wind tunnel is closed with a maximum velocity of 60m/s. The dimension of the measuring section is 2m long, 0.7m high and 0.7m wide. The model was attached to a three component dynamometer and available to adjust the ground clearance and the angle of attack. The acrylic plastic board bisected the measuring section and was used as the ground as shown in fig. 3. The wind velocity varied from the wall and the ground as shown in Fig. 4, so the boundary layer was estimated at 3 cm from the ground.
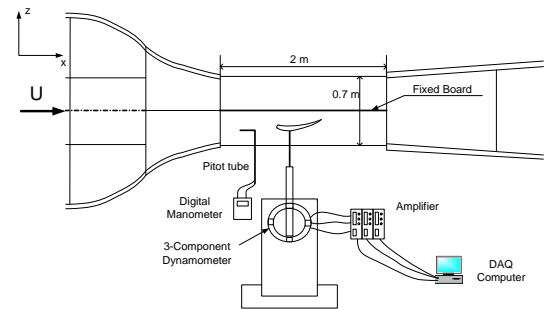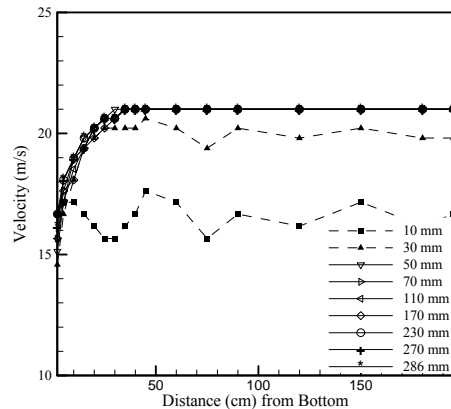

Fig. 3. Measuring system in the wind tunnel

Fig. 4. Velocity distributions from wall in wind tunnel

The DHMTU (2.65-20, 1.818-40, 1.515-60, -4.5 3) wing was used for the wind tunnel test. The DHMTU section had an s-shaped mean line as shown in Fig. 5. The aspect ratios of these wings were 1.0. Two endplates were used in order to investigate the endplate's influence on the ground effect. Type A and B endplates had heights of 0.05c and 0.1c, respectively, from the trailing edge of the wing as shown in Fig. 5. The bottom of the endplate was kept parallel with the ground even though the wing's angle of attack changed. The ground clearance h was the distance from ground to the trailing edge of the wing without an endplate and to the bottom of the endplate for a wing with an endplate.

Fig. 5. Configuration of wing and endplate type A and B

4. Results

Fig. 6 represents the results of the grid sensitivity test for the lift coefficient of a planar wing (aspect ratio=1.0). These results show that the simulation using the vortex grid of 4 chordwise and 13 spanwise on the wing converged with a planar wing. Based on this result, the 4×13 grid system was used for the planar wing with a unit aspect ratio, and the number of the spanwise grid was adjusted with each aspect ratio. The DHMTU wing was simulated by the 10×10 grid because it had the S-type of cross section with a thin thickness as shown in Fig. 5. The numerical model using the Vortex Lattice Method (VLM) simulated the wing geometries in which the wing section, aspect ratio, endplate shape, sweep angle, and taper ratio were varied. Also, it was applied to the WIG craft model including the main and tail wings and subsequently compared to the experimental results.

Two (A and B) endplates shown in Fig. 5 were used to investigate the endplate effect in the vicinity of the ground. The ground clearance (h/c) was defined as the distance between the ground to the trailing edge of wing for cases without endplate and to the bottom of endplate for cases with endplate as shown in Fig. 5.

The spanwise lift loading (C_l) distribution for various planar wing sweep angles and taper ratios are presented and subsequently compared to Katz's (1985) results in Fig. 7 and Fig. 8. Those results agree well for swept and tapered wings. The lift loading of the forward swept wing (Λ=135°) was larger at the wing-root (2y/b=0), but the aft swept wing (Λ=45°) had larger lift loading at the wing-tip (2y/b=1.0). At the structural point of view, the bending moment at the wing-root was smaller for the forward swept wing than for the aft swept wing. Because the stall initiates at the wing-root section for the forward swept wings, the forward swept wing is expected to have less rolling moment due to the stall phenomena locally occurring on the wing surface. The taper ratio (λ) is defined as the ratio of chord lengths at wing-tip and wing-root.
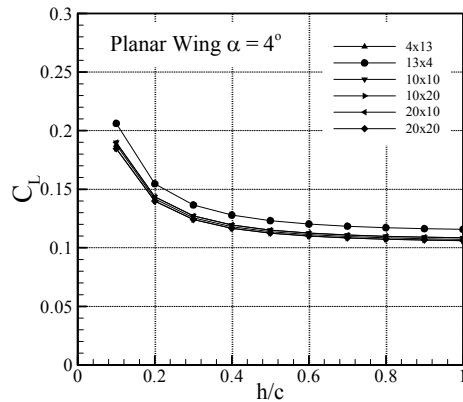
$$\lambda = \frac{c_{y=b/2}}{c_{y=0}}$$

(16)

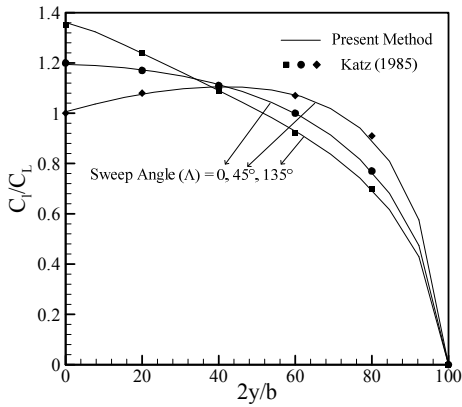Fig.6 Grid sensitivity in lift coefficient of planar wing

Fig. 7. Spanwise loading of planar wing (AR=4, =4) with 3 sweep angles
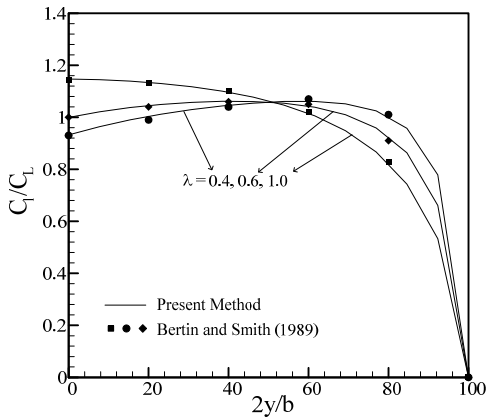

Fig. 8. Spanwise loading of untwisted wing (AR=7.28, =5) with 3 Taper Ratios

Fig. 8 shows that the local lift coefficient, non-dimensionalized by the local chord length instead of the wing area, increased at the wing-tip with smaller taper ratio.

The lift coefficients using the VLM were compared to the experimental results (Fink and Lastinger, 1961) and numerical results using VSAERO (Maskew, 1982) for Glenn Martin 21 percent thickness non-symmetric wing section. Fink and Lastinger (1961) performed the experiments using the image-wing method to eliminate the boundary layer between the wing and the ground in the wind tunnel.

Because the VLM did not include the wing thickness distribution along the wing chord, VLM results were possibly overestimated at low ground clearances as shown in Fig. 9. The lift to induced drag ratio for a rectangular wing having the maximum camber equal to 4% of chord length is compared with numerical results (Day and Doctors, 1995). These results demonstrated good agreement in Fig. 10 for the ground effect.
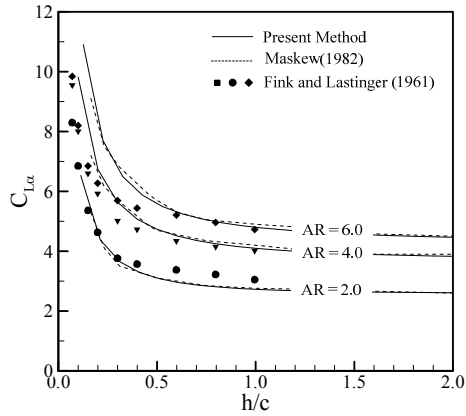

Fig. 9. Effect of ground proximity on the CL of rectangular wings
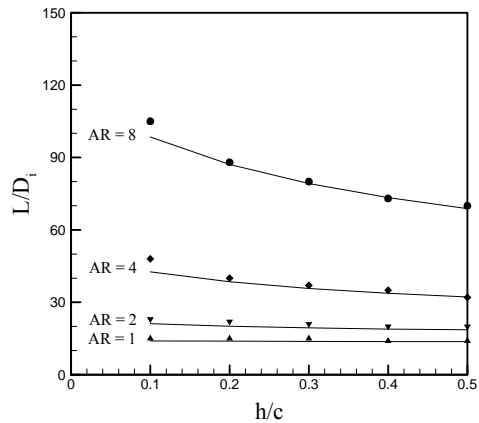

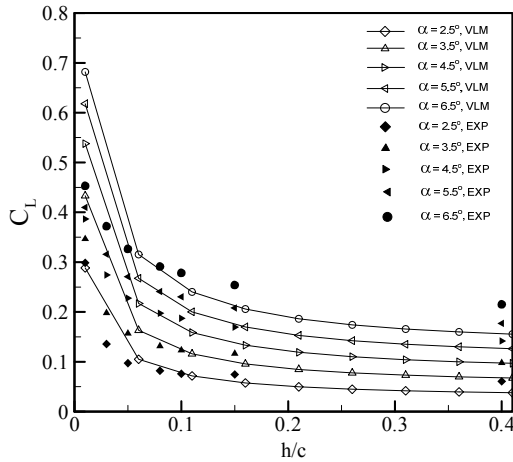Fig. 10. Lift to drag ratios for rectangular wing of 4% maximum camber
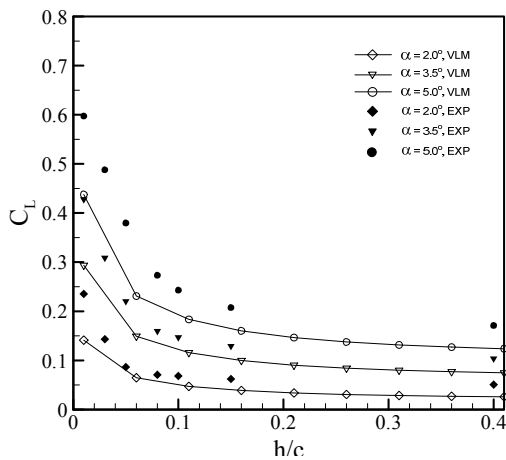
Fig. 11(a). Without endplate
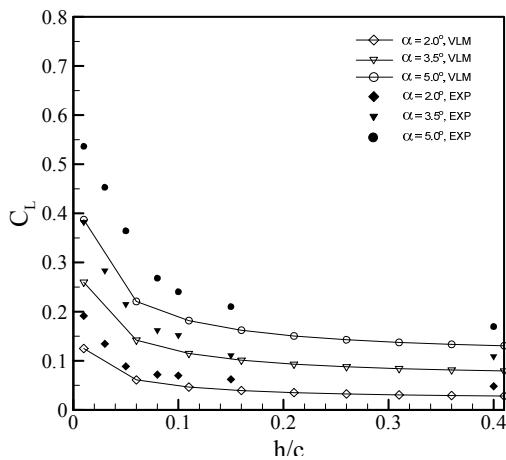

Fig. 11(b). With endplate A

Fig. 11(c). With endplate B
Fig. 11 Lift coefficient (CL) variation of DHMTU wing with h/c

The DHMYU wing series were developed for the utmost ground effect, which has a thin thickness and S-type cross section.   The DHMTU (2.65-20, 1.818-40, 1.515-60, -4.5 3) has the 4% thickness of chord length as shown in Fig. 5.   The numerical results using the VLM were compared to the experimental data acquired from the wind tunnel experiments. Fig. 11 shows that the lift coefficient (C_L) increased due to the ground effect with reducing ground clearance (h/c).   In the comparison between numerical and experimental results, the lift coefficient of the numerical results overestimated that of experimental results except for the case without an endplate (W/O) when very close to the ground (h/c<0.1).   Because the experimental cases for   low ground clearance (h/c<0.1) without the endplate (W/O) were measured within the boundary layer of the wind tunnel, which was about 3cm (h/c=0.1), the wind velocity within the boundary layer was slower than out of the boundary layer (h/c>0.1) as shown in Fig. 4.   In cases with endplates (W/A and W/B), the wing was more separated from the ground (the wind tunnel bottom) by amounts similar to the endplate heights (W/A=0.05c and W/B=0.1c).   Therefore, the lift coefficients of the low ground clearance cases without an endplate were underestimated in the wind tunnel test. Both numerical and experimental results represent the endplate effect in which the lift coefficient increased due to the reduction of the vortex separated from the trailing edge. Chun et al (1996) presented the endplate effect using the smoke trace technique for the flow visualization in the wind tunnel.
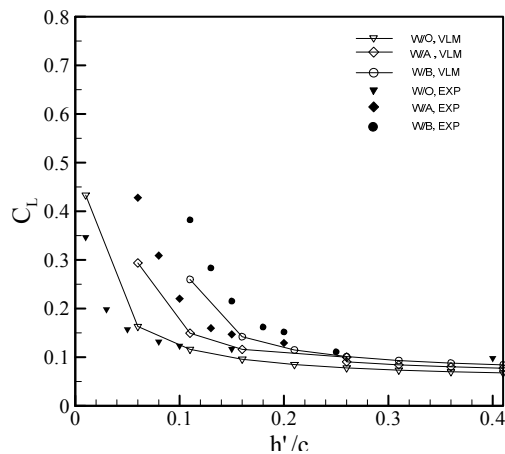

Fig. 12. Lift Coefficient (CL) variation of DHMTU wing with h′/c   (=3.5)

In Fig. 12, the ground clearance was defined from the wing trailing edge to the ground for cases W/O, W/A, and W/B which is denoted by h′/c as shown in Fig. 5. The lift coefficients are represented as functions of the distance (h'/c) from the trailing edge to the ground, which shows the lift coefficients increasing due to endplate (W/A and W/B) effect near the ground. At h'/c=0.1, for example, the lift coefficient for W/B case was approximately 2~3 times greater than that for the W/O case, which was the endplate effect augmenting the lift force at the small ground clearance. Note that the C_L lines of W/A and W/B were similar to that of W/O for the ground clearance from the lower edge of endplates. The endplate's height and shape must be optimized in order to enhance the ground effect with the consideration of the operation stability of WIG craft to avoid touching the free surface at the cruise condition.
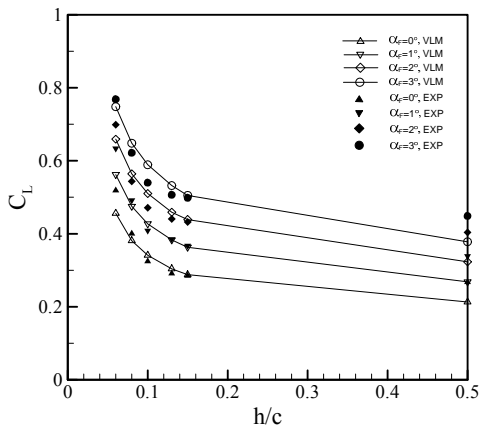

Fig. 14(a). Side view

Fig. 14(b). Oblique view

Fig. 14(c). Back view

Fig. 14. Wake roll-up of a rectangular wing at a sudden acceleration AR = 1.0, =5o

Fig. 13. Lift Coefficient (CL) variation of 20 passenger WIG craft

Fig. 13 shows the comparison of the lift coefficients using the VLM and wind tunnel test for the 20 passenger WIG craft at differing angles of attack (α_F) of the fuselage. The model geometry is added in Table 1 with the model scale. The numerical model for 20 passengers WIG was simplified into two parts: the main wing and tail wing. This simplification was made because the VLM did not compute the thickness effect of the fuselage and wing body. These results correlated fairly well with the experimental results in the wind tunnel, which indicates that the VLM simulated the wake separated from the main wing affecting to the tail wing well.
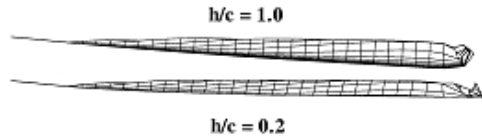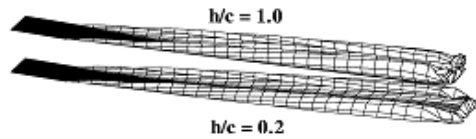
The wake deformation of the planar wing due to the ground effect is represented in Fig. 14. The force free vortex wake was assumed to be separated only at the trailing edge. When the wing was placed at h/c=1.0, the back view of the rolled-up wake was shaped in the parabolic curve below the wing and the wake separated at the trailing edge was coiled into the mid-span of wing. With the ground effect (h/c=0.2), however, the wake that separated from the trailing edge formed parallel to the ground and spread out of the wing-tip due to the reflection on the ground.

5. Conclusion

The Vortex Lattice Method (VLM) was employed for various wing-in-ground effect geometries. The numerical results using the VLM correlated well with the numerical and experimental results obtained by different techniques. VLM was applied to inves-

tigate the aerodynamic characteristics of the DHMTU (2.65-20, 1.818-40, 1.515-60, -4.5 3), which has 4% thickness of chord length, in the ground effect. The endplate attached to the wing tip augmented the ground effect, which increased the lift force and improved the aerodynamic efficiency (lift-to-drag ratio). Lift coefficients with endplate types A (W/A) and B (W/B) have similar magnitudes over various clearances (h/c) even though the endplates were positioned at different distances from the ground to the trailing edge of wing. Because the distance between the ground and the trailing edge of the wing was important to the stability, the endplate's height and shape should be considered as design parameters in order to optimize the aerodynamic efficiency of the WIG craft with the operational stability at the cruising condition. VLM simulated the wake deformation due to the ground effect, which was reflected on the ground and spread in the spanwise direction. This wake deformation due to the ground effect resulted in increasing the effective aspect ratio of the wing. In addition, the VLM model was used to simulate the WIG craft model conceptually designed to carry 20 passengers with the VLM. These numerical results agreed well with experimental results from the wind tunnel test. Therefore, the vortex lattice method was capable of calculating the aerodynamic forces including the ground effect and the endplate and performing a reasonable aerodynamic parametric study at the conceptual design stage with less computational time compared with other inviscid and viscous numerical methods. In addition, the VLM could analyze the characteristics of the longitudinal static height stability, which is of prime importance in a safe WIG design including the effect of the tail wing on the height stability. This study presented the VLM as a capable method for evaluating the aerodynamic characteristics for various wing shapes, the ground effect with endplate, and the 20 passenger WIG craft.

References

[1] Ahmed, M.R. and Sharma, S.D., *An Investigation on the aerodynamics of a symmetrical airfoil in ground effect*, Experimental Thermal and Fluid Science vol. 29, (2005) 633-647.

[2] Carter, A.W., *Effect of Ground Proximity on the Aerodynamic Characteristics of Aspect Ratio 1 Airfoils with and without Endplates*, NASA TN D-970,(1961).

[3] Chun, H.H. and Chang, C.H., *Longitudinal stability and dynamic motions of a small passenger WIG craft*, Ocean Engineering vol. 29, (2002) 1145-1162.

[4] Chun, H.H., Chang, C.H., Paik, K.J., and Chang, S.I., *Preliminary Design of a 20 Passenger PARWIG Craft and Construction of a 1/10 Scale Radio Controlled Model*, Proceedings of FAST'97, Sydney, July, (1997)513-519.

[5] Chun, H.H., Chung, K.H., and Chang, J.H. *Smoke Trace Flow Visualization of a Wing in the Vicinity of the Ground*, 2nd Japan-Korea Joint Symposium on Advanced Technologies, Yokohama National University, Japan, Oct. 31~Nov. 2, (1996) 285-298.

[6] Day, Alexander H. and Doctors, Lawrence J., *A Study of the Efficiency of the Wing-In-Ground-Effect Concept. Proceedings* of Workshop on Twenty-First Century Flying Ships, Nov, (1995) 1-22.

[7] Fink, P. M., and Lastinger, L. J., *Aerodynamics Characteristics of Low-Aspect-Ratio Wings in Close Proximity to the ground*, NASA TN D-926 (1961).

[8] Fuwa, T., Takanashi, N., Hirata, N., and Kakugawa, A., *A Study on the Conceptual Design of Wing in Surface Effect Ships. Proceedings of 6th International Symposium on Practical Design of Ships and Mobile Units*, Society of Naval Architects of Korea, Seoul, Korea, September 17 - 22, (1995) 1735 - 1746.

[9] Halloran,M. and O'Meara,S., *Wing in Ground Effect Craft Review*, DSTO Aeronautical and Maritime Research Laboratory, DSTO-GD-0201, Australia, (1999).

[10]Hess, John L., *Calculation of Potential Flow about Arbitrary 3-D Lifting Bodies*, Report No. MCD J5679-01, McDonell Douglas, Oct, (1972).

[11]Jung, K.H., Chun, H.H., and Kim, H.J., 2008, *Experimental investigation of wing-in-ground effect with a NACA6409 section*, Journal of Marine Science and Technology, Vol. 13, No.4, In printing (2008).

[12]Kang, K.J., *Twenty Passsenger Class Wing in Ground Craft. Proceedings of the Annual*

Autumn Meeting, SNAK, Yongin, Korea, Nov, (2005) 958-971. (in Korean)

[13] Katz, J., *Calculation of the Aerodynamic Force on Automotive Lifting Surface. ASME Journal of Fluids Engineering*, vol. 107, (1985) 438-443..

[14] Kirillovikh V.N., *Russian Ekranoplans*, Proceedings of Workshop on Twenty-First Century Flying Ships, Sydney, Australia, (1995) 71-117.

[15] Konstadinopoulos, P., Thrasher, D.F., Mook, D.T., Nayfeh, A.H., and Watson, L., *A Vortex-Lattice Method for general, Unsteady Aerodynamics,* Journal of aircraft, vol. 22, NO. 1, (1985) 43-49.

[16] Kubo, S., A Production Model of WIG *as a High Speed Marine Craft: 'Marine Slider - Sky 2,* Proceedings of FAST 91, Trondheim, Norway, (1991) 607 - 622.

[17] Kuehmstedt, T., *Aerodynamic Design Procedure and Results of the Development of Commercial WIG Craft*, Proceedings of Ekranoplans & Very Fast Craft, University of New South Wales, Sydney, Australia, 5-6 December, (1996) 20-37.

[18] Maskew, B., Program VSAERO, *A Computer Program for Calculating the Nonlinear Aerodynamic Characteristics of Arbitrary Configurations*, NASA CR-166476, Nov, (1982),

[19] Ming, L.S., Xai, L.K., Hua, Y.C., Bo, N., and Nai, Y.X., *Development of Wing-in-Ground Effect in CSSRC*, Proceedings of Workshop on Ekranoplans & Very Fast Craft, The University of New South Wales, Sydney, Australia, December 5-6, (1996) 244-257.

[20] Muzitani, N. and Suzuki, K., *Numerical Analysis of 3-D WIG Advancing over Still Water Surface*, Journal of the Society of Naval Architects of Japan, Vol. 174, December , 35-46 (in Japanese), (1993).

[21] Nuhait A. O. and Mook, D. T., *Numerical Simulation of Wings in Steady and Unsteady Ground Effects*, Journal of aircraft, vol. 26, NO. 12, Dec., (1989)1081-1089.

[22] Shin, M.S., Yang, S.I., Joo, Y.C., Kim, S.K., Bae, Y.S., Kim, J.H., and Chun, H.H., *Wind Tunnel Test Results for Eight and twenty Passenger Class Wing in Ground Effect Ships*, Proceedings of FAST'97, Sydney, July, (1997) 565-570.

[23] Sinitsyn D.N.,*Summary of the Construction of the First Commercial Ekranoplan, Amphistar. Proceedings of Workshop on Ekranoplans & very fast Craft*, The University of New South Wales, Sydney, Australia, December 5-6, (1996) 146-151.